Dedicated to Acad. Aureliu Săndulescu's 75th Anniversary

INVESTIGATION OF DISSIPATIVE COLLISIONS WITH TRANSPORT MODELS

T. MIKHAILOVA[1], M. COLONNA[2], M. DI TORO[2], H. H. WOLTER[3]

[1] JINR, Dubna, Russia. E-mail: tmikh@nusun.jinr.ru
[2] LNS-INFN, Catania, Italy
[3] Dep. of Physics, University of Munich, Germany

Received March 27, 2007

Deep Inelastic Collisions (DIC) were investigated at energies around the Coulomb barrier. They attracted renewed attention, when it was found that the same mechanism exists also at energies of the order of the Fermi energy. In this type of collisions one may investigate the dissipative properties of nuclear matter. In the past, the theoretical description of this mechanism was given mainly in terms of classical models which explicitly include friction. Here we use the transport approach of the Boltzmann-Nordheim-Vlasov (BNV) type to describe peripheral nucleus-nucleus collisions at Fermi energies. We applied these to experimental results of ^{18}O on ^{181}Ta and ^{9}Be collisions at $E/A = 35$ MeV. We calculate deflection curves, Wilczynski plots, velocity and isotope distributions of light fragments. We suggest that the experimental data in addition to the dissipative process contain contributions from a direct breakup, which is described in the Goldhaber model. With the transport calculations we explain rather well the features of the dissipative contribution.

1. INTRODUCTION

Deep Inelastic Collisions (DIC) occur when heavy ion collide around the grazing impact parameters where the exit channel is still essentially binary. The process thus lies between fusion-fission reactions which correspond to more central collisions and peripheral collisions which involve only few nucleon degrees of freedom. Damped or Deep-Inelastic Collisions are characterized by substantial kinetic energy damping and mass exchange, while retaining partial memory of entrance-channel masses and charges. They have been extensively studied in the past in the Coulomb energy range in order to investigate the dissipative properties of nuclear matter [1]. There have been different approaches for their theoretical description, which are reviewed, *e.g.*, in the reports of H. Fuchs and K. Möhring [2] and of U. Schroeder and J. R. Huizinga [3]. Well known is the interpretation in terms of a classical friction model by Gross *et al.* [4]. This approach was very successful in explaining a large amount of experimental data,

but contained empirical friction coefficients. A more microscopic approach, Dissipative Diabatic Dynamics, was introduced by Nörenberg *et al.* [5]. It used the two-center shell model and the Landau-Zener theory for the treatment of level crossings. In the last years the interest in DIC has revived when it was found that this type of reaction has appreciable cross-sections also at energies of the order of Fermi energy.

In the Fermi energy regime, the velocities of the collective motion of the nuclei and the Fermi motion of the nucleons are of the same magnitude. Therefore processes should occur, which are mediated by direct NN-collisions and where the mean field is of lesser importance, such as direct and breakup processes. It will be of interest to see the evolution of the importance of these different reaction mechanisms.

Here we apply the Boltzmann-Nordheim-Vlasov (BNV) transport approach (also named Boltzmann-Uehling-Uhlenbeck approach, BUU) [6] to describe DIC in the Fermi energy regime. This approach has been used extensively in the last decades to describe higher energy heavy ion collisions. It was also applied earlier for DIC, *e.g.* by Rivet *et al.* [7] for the reaction Ar + Ag at E/A = 27 MeV, and gave a quantitative agreement with the experiment. Because of calculational restrictions of that time it was not possible to make detailed predictions concerning velocity and isotope distributions. Now full calculations taking into the account the whole range of impact parameters involved in the reaction are possible.

In this investigation we were motivated by the experimental results for peripheral collisions of ^{18}O on ^{181}Ta and ^{9}Be at 35 MeV per nucleon measured at forward angles by the Artukh group in Dubna [8, 9]. In these papers experimental data on charge, isotope and velocity distributions for these two reactions were presented. In addition, in ref. [9] the measured distributions were compared extensively with calculations in the Quantum Molecular Dynamics (QMD) model. Good agreement was obtained for charge and isotope distributions, but the model failed to explain the velocity distributions, which experimentally are peaked at the beam velocity. It will be shown that we find similar results. However, in our interpretation the experimental data contain two contributions, a direct breakup and a dissipative contribution, as discussed above. After extracting the direct component we find reasonable agreement of the calculations with the dissipative component.

In fact, a similar experiment was performed earlier by Lahmer *et al.* [10], where fragmentation of a ^{14}N beam of 60 AMeV was measured from targets between ^{12}C and ^{208}Pb. The precisely measured isotopic fragment energy spectra were similarly decomposed into a breakup (fragmentation) and a dissipative component by Gaussian fits, where the latter was described successfully by models of Goldhaber [11] and of Utsonomiya [12]. Fragmentation at lower energies was also measured by Gelbke *et al.* [13].

The paper is organized as follows: In the next section we give a brief summary of the transport model, as well as of the fragment recognition mechanism. In Sect. 3 we discuss the results of the theoretical calculations in terms of deflection curves, Wilczynski plots, and isotope and velocity distributions. Finally in Sect. 4 we compare to the experimental results of ref. [9]. Here we will argue that the data contain two contributions, of which in our theoretical calculations we only describe the dissipative one.

2. DESCRIPTION OF THE TRANSPORT MODEL

The BNV transport approach describes the time evolution of the one-body phase space distribution function $f(\mathbf{r}, \mathbf{p}, t)$ under the influence of a mean field $U(f)$ and a Boltzmann two-body collision term I_{cls}, which includes the effect of Pauli blocking (Nordheim or Uehling-Uhlenbeck collisions term) [6, 14]

$$\frac{\partial f}{\partial t} + \frac{\vec{p}}{m}\nabla_{\vec{r}} f - \nabla_{\vec{r}} U \nabla_{\vec{p}} f = I_{cls}. \tag{1}$$

Here m is the nucleon mass. The potential $U(f)$ used in our calculations is the sum of the Coulomb potential and a mean field potential of the Skyrme type [15].

The solution of the integro-differential equation (1) is obtained by simulations using the test-particle method. The distribution function $f(\vec{r}, \vec{p}, t)$ is represented as a sum of contributions of test particles, distributed over the volume of the system, having velocities in the local Fermi sphere:

$$f(\vec{r}, \vec{p}) \cong \frac{1}{NA} \sum_i g(\vec{r} - \vec{r}_i(t))\, \tilde{g}(\vec{p} - \vec{p}_i(t)). \tag{2}$$

The quantities $\vec{r}_i$, $\vec{p}_i$ are the position and momentum of test particle i, moving in time, and the functions g and $\tilde{g}$ describe the shape of a test particle distribution in coordinate and momentum space. N is the number of test particles per nucleon; thus the distribution function for a nucleus of mass A is represented as a sum of NA test particles. Test particles also carry an index for isospin, such that protons and neutrons can be distinguished. It can be shown that between collisions the test particles propagate according to Hamilton equations of motion

$$\begin{aligned} \vec{p}_i(t + \Delta t) &= \vec{p}_i(t) - \Delta t\, \nabla_r U(\vec{r}_i, t) \\ \vec{r}_i(t + \Delta t) &= \vec{r}_i(t) + \Delta t\, \vec{p}_i/m. \end{aligned} \tag{3}$$

Often the shapes of the test particles are taken as δ-functions. However, the smoother the distribution function the better is the approximation to the solution

of the original kinetic equation. For this reason often more general functions of finite extent, as *e.g.* Gaussians as in our case, are used. The smoothness of the distribution function is determined by the number N and by the widths σ_R and σ_P of the test particle shape functions. However, the widths are not completely free parameters as they are determined by surface thickness and stability of the initial nucleus. The number of test particles per nucleon, N, can be varied. Since it controls the smoothness of the distribution function, it also determines the amount of numerical fluctuations. Fluctuations become important in regions of instability, as *e.g.* in fragmentation. Thus the test particle number has often been used to investigate the role of fluctuations in transport calculations.

The collision term is treated in a stochastic way. After each time step Δt in Eq. (3) (or several time steps, depending on the accuracy) it is checked, whether test particles undergo collisions. The criterion for the collision to take place is that the distance between two test-particles should become less than $\sqrt{\sigma/\pi}$. Here σ is the total collision cross-section, which is taken as $40mb$ in our case. Pauli blocking is taken into account when determining the final momenta of the colliding test particles.

To start the solution of the set of eqs. (3) the initial conditions of the mass and charge of the colliding nuclei, their kinetic energies and impact parameters are initialized. The time evolution of the set of $\vec{r}_i$ and $\vec{p}_i$ is calculated for all test particles. The positions of r_i and p_i determine the distribution function $f(r, p, t)$, and the equations

$$\begin{aligned} n(r,t) &= \int f(r,\, p,\, t)\, d\vec{p} \\ \vec{u}(r,t) &= \frac{1}{m} \int \vec{p}\, f(r,\, p,\, t)\, d\vec{p} \end{aligned} \tag{4}$$

give the local number density $n(r, t)$ and mean collective velocity $\vec{u}(r, t)$ of the distribution.

The time evolution of the test particles is continued until some critical point which we call freeze-out point (about 150 fm/c for peripheral reactions). The freeze-out time is determined as the one, at which the distance between the two fragments in the exit channel is large enough so that nuclear forces become negligible. At this point the calculation is stopped. At freeze-out the state of the system can be characterized as a collection of primary fragments. In the case of DICs, which are essentially binary, there are the projectile-like fragment (PLF) and the target-like fragment (TLF) and in addition some smaller emitted light particles, mainly single nucleons. One has to employ a cluster recognition algorithm to identify the fragments. Mostly coalescence model are used for this. In this work we used a simple cut-off method in coordinate space. The boundary of a fragment is determined by a cut-off density n_m, taken here as 1/8 of the

saturation density n_0. The proton and neutron number of the cluster is determined by integrating over the proton and neutron test particle distributions inside the boundary. These numbers are generally non-integer, because a test particle represents only $1/N^{th}$ of a nucleon. If *e.g.* the charge is $Z_0 + \zeta$; $0 < \zeta < 1$, where Z_0 is integer, then we assume charge Z_0 with probability $1 - \zeta$ and charge $Z_0 + 1$ with probability ζ, and similarly for the neutron number. It was checked that the results do not differ very much, if more elaborate algorithms are used, which also take into account the momentum space. It is clear that the so-called primary fragments generated in this way are still excited. In principle a de-excitation code should be employed to describe the secondary evaporation and to obtain the final cold fragments observed in experiment. This has not yet been done in this work, and is discussed later on.

For each of the fragments we then find the coordinates of the center of mass, and the velocity of the fragment i as

$$\begin{aligned} \vec{R}_i &= \int \vec{r}\, n(r,t)\, d\vec{r} \\ \vec{V}_i &= \int \vec{u}(r,t)\, n(r,t)\, d\vec{p}, \end{aligned} \tag{5}$$

and similarly other physical properties of the fragments. From positions of the fragments and their velocities at freeze-out Coulomb trajectories are determined in order to find the asymptotic angles and kinetic energies of the fragments. To facilitate the comparison of the results of the calculation with experiment all velocities are transformed from the center of mass to the laboratory system.

In this way for each simulation run the mass numbers A and charges Z of the fragments, their velocities $\vec{V}$ and directions of movement (angles in the laboratory system) are calculated. In principle, the kinetic equation is deterministic, but the way of treating the collision term introduces stochastic features. Calculations with the same initial conditions give results with slightly varying values of the properties of the fragments. A large number of "events" has to be calculated to obtain reasonably smooth distributions.

The only changing initial parameter in our calculations is the impact parameter b of the collision. To simulate the conditions of the experiment calculations with a set of impact parameters from b_{min} to b_{max} were preformed. The value of b_{min} corresponds to the transition from fusion to the binary deep inelastic process, and is taken 2 fm for the reaction $^{18}O + {}^{9}Be$ and 7 fm for $^{18}O + {}^{181}Ta$, while the upper limit b_{max} was chosen in such a way that the two nuclei do not form a composite system even for a short period of time (7 fm for the reaction with the light target and 11 fm for the heavier target). To have good statistics on the average 50 runs of the code for each value of b were performed.

To make it possible to compare the calculations for different impact parameters all the physical quantities were then normalized by the number of runs giving the probability for one event.

If Φ_i is the distribution for some quantity (*e.g.* mass A, charge Z, velocity, or angular distribution) for a given value of the impact parameter b_i, then the total yield of this quantity is found as

$$\Phi_{tot} = \pi \sum_{i}^{N_b} (b_{i+1} + b_i)(b_{i+1} - b_i)\Phi_i \,.$$

The results of the theoretical calculations are discussed in the next section and the comparison with the experiment will be discussed in Sect. 4.

3. RESULTS OF CALCULATIONS

We show results of calculations for the two reactions $^{18}O + {}^{9}Be$ and $^{18}O + {}^{181}Ta$ at 35 AMeV energy beam, measured in refs. [9, 8]. The calculations were done with a potential of Skyrme type with a stiff equation-of-state [15]. We used 200 test-particle per nucleon for the reaction $^{18}O + {}^{9}Be$, and 50 and 100 test-particles per nucleon for $^{18}O + {}^{181}Ta$ to see the influence of this parameter, *i.e.* of fluctuations, on the final results. Usually we calculated 50 events for each case. As in the experimental paper the distributions at forward angles were studied, in particular. (In the experiment [8] the measurements were done for an acceptance angle $\theta < 2.5°$). To study which impact parameters give their contribution into emission of light particles at forward angles the deflection curves, *i.e.* mean laboratory deflection angles of the projectile like fragments (PLF) in the lab system as a function of the impact parameter, were calculated. As one can see these calculations were done for much larger region of impact parameters than was necessary to obtain velocity and isotope distributions.

Deflection curves for the two reactions $^{18}O + {}^{9}Be$ and $^{18}O + {}^{181}Ta$ at projectile energy $E_0 = 35$ AMeV are shown in Figs. 1 and 2 respectively. The experimental acceptance angle is shown as the dashed area. The vertical line marks the impact parameter equal to the sum of the radii $R_1 + R_2$. The dash-dotted line is the deflection curve for classical Rutherford scattering for point-like Coulomb forces only. The Coulomb rainbow for large impact parameters is seen in both cases, while the nuclear rainbow is also evident for the light target.

The contributions to the scattering at forward angle are qualitatively different in the two reactions. The case of the light target ^{9}Be (Fig. 1) corresponds essentially to inverse kinematics. Here most contributions at forward angles correspond to Coulomb trajectories or trajectories slightly inside the Coulomb

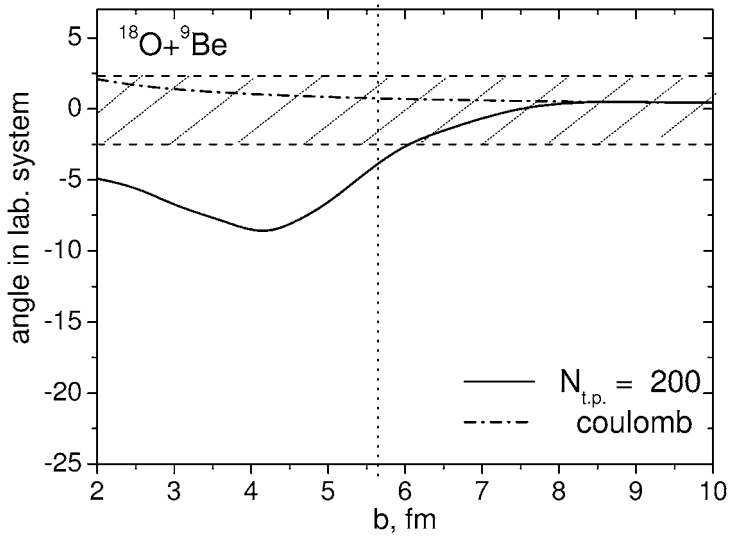

Fig. 1 – Deflection curve, *i.e.*, mean laboratory deflection angles of the projectile-like fragments (PLF) in the lab system as a function of the impact parameter, for the reaction ^{18}O + ^{9}Be, calculated with 100 test particles per nucleon. The dashed region corresponds to the acceptance angle of the experiment of ref. [8]. The sum of the nuclear radii is indicated by the vertical dashed line. Also shown is the pure Coulomb deflection curve.

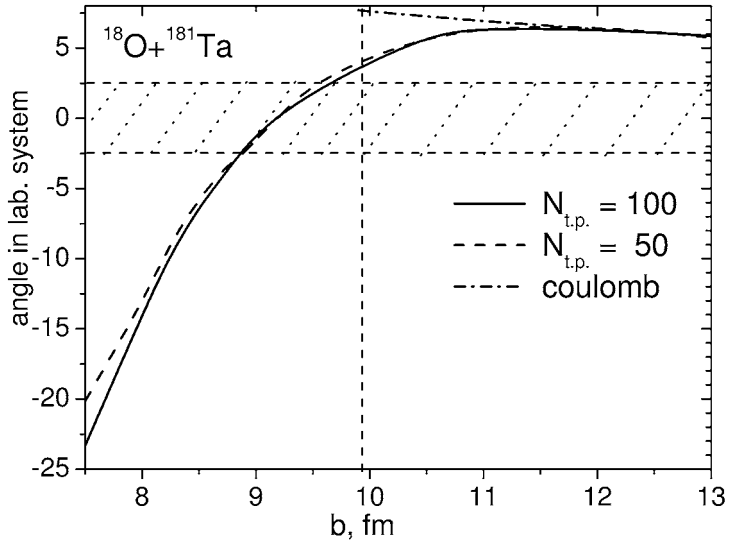

Fig. 2 – Deflection curves for the reaction and ^{18}O + ^{181}Ta, as in Fig. 1. Results of calculations with 50 and 100 test particles per nucleon are shown.

rainbow. Here we expect very little dissipation at forward angles. In contrast, the heavy target ^{181}Ta (Fig. 2) corresponds to normal kinematics. Here the trajectories at forward angles correspond to deeply diving trajectories inside the sum of the radii, and we expect pronounced dissipation effects. For the latter reaction calculations with different numbers of test particles are shown. As it is expected the fluctuations have little influence on these global quantities. The different behavior of deflection curves reflects the difference between the normal and inverse kinematics. We will mainly present the calculations for the reaction on ^{181}Ta as a target because of its greater interest in studies of dissipation.

The dissipative character of a DIC has often been studied in terms of the dependence of energy loss on deflection angle. A contour plot of the constant cross section in the deflection angle and kinetic energy plane is called Wilczynski plot [1]. In Fig. 3 we show this dependence for the reaction ^{18}O + ^{181}Ta. The energy represented here is the final kinetic energy divided by the initial kinetic energy in center of mass system. It demonstrates the rather strong correlation of the energy loss with the deflection angle and consequently the impact parameter, and thus shows that our approach reproduces nicely the main features of deep inelastic collisions. The lower branch of the curve corresponds to negative deflection angles relative to the beam axis, *i.e.* orbiting. The notion of 'orbiting' is usually connected with 'friction'. The contours are plotted separately for the contributions of different *Z*. This shows also the correlation between energy and mass loss.

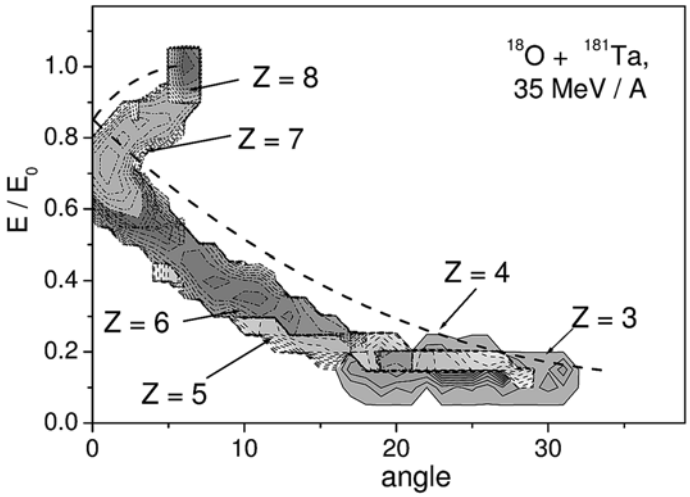

Fig. 3 – Wilczynski plot for the reaction ^{18}O + ^{181}Ta: Contour plot of constant cross sections for PLF of different *Z* in the plane of deflection angle and kinetic energy in the center of mass system relative to the initial projectile energy E_0. Negative deflection angles are flipped to the positive side. Dashed line shows estimate for energy loss due to rotational energy of the target-like fragment (see text).

A part of the energy dissipated in the reaction is transformed into excitation energy while the other part could be transformed into other types of collective motion. To investigate this we show in Fig. 4a Wilczynski plot similar to Fig. 3 but for a solution of the kinetic equation, eq. (1), without collision term. (In this figure we have not flipped the negative angles to positive ones.) The energy loss is seen to be smaller than in Fig. 3 but still substantial, however, the width of the distribution is much smaller for calculations without collision term. The fact, that we observe energy dissipation in transport calculations without a collision term is expected: firstly, we approximate the smooth distribution function with the sum of test particles and this coarse graining of the distribution leads effectively to dissipation [16], and secondly, the collision term determines two-body dissipation, but there also exists mean field or one-body dissipation [17]. We see here that the fluctuations are reduced in the absence collisions, leading to the smaller width of the distribution.

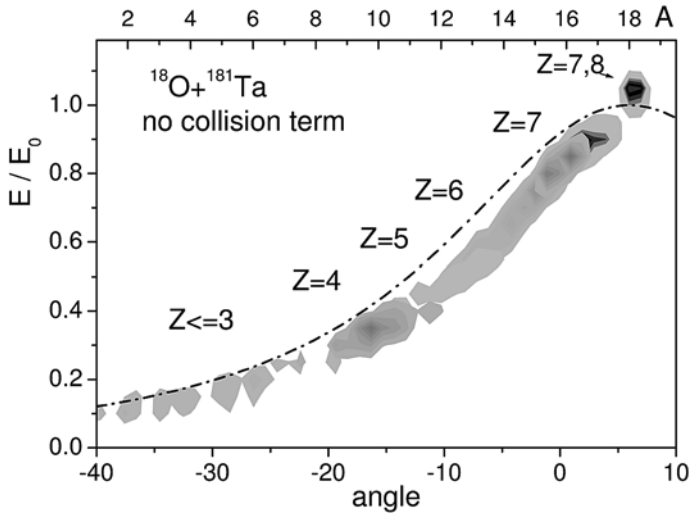

Fig. 4 – Wilczynski plot for the reaction ^{18}O + ^{181}Ta as in Fig. 3 for the solution of the kinetic equation without collision term. Here negative deflection angles are shown.

As a simple model for the energy transfer into collective motion we estimate the contribution of rotational energy which is transferred into the target-like fragment, which absorbs the mass $A_K = A_P - A_{PLF}$. The dashed curves in Figs. 3 and 4 show this rotational energy, which is calculated as $E_{rot} = M^2/(2J_T)$, where the angular momentum is $M = (A_K)mb$ and the moment of inertia $J_T = (2/5A_T + A_K)mR_T^2$ ($A_T m$ and $A_T m$ the mass of target and projectile nuclei respectively, R_T radius of target, $A_{PLF}m$ mass of the PLF). It is seen that it

underestimates the energy loss curve in Fig. 4 only slightly, while the additional dissipation into excitation is seen clearly in Fig. 3. It is thus seen that the rotational energy accounts for a substantial part of the transferred energy.

A more detailed view of the energy dissipation mechanism is obtained by studying also the mass loss, *i.e.* the isotope distributions, and the velocity distributions of the PLF. In fact, this was also what was studied mainly in ref. [9]. Of course, these isotope and velocity distributions depend strongly on the impact parameter b of the collision and thus also of the acceptance angle of the detector.

In Fig. 5 isotope distributions for PLFs for the reaction $^{18}O + ^{9}Be$ are presented: in the upper part the distributions for fragments emitted into all forward angles and in the lower part the distributions with the restriction of the experimental acceptance angle $\theta < 2.5°$. The same is shown in Fig. 6 for the reaction $^{18}O + ^{181}Ta$, in this case, however, for the two calculations with 50 (dashed curves, open symbols) and 100 (solid curves, full symbols) test particles per nucleon. It is seen that only fewer and heavier fragments are observed and that the distributions are narrower when the acceptance angle is restricted. This is evident, since from the deflection curves in Figs. 1, 2 we know, that the angle restriction limits the range of impact parameters to larger values, where less mass can be transferred. It is also seen in Figs. 5 and 6, that the range of PLF isotopes is much smaller for the lighter ^{9}Be target, since the surface is much smaller and thus the overlap smaller and the interaction time shorter. It is also seen that the width increases for lighter fragment masses, *i.e.* when more mass is lost, which again is due to the longer interaction time [3]. Finally in Fig. 6 in the calculation

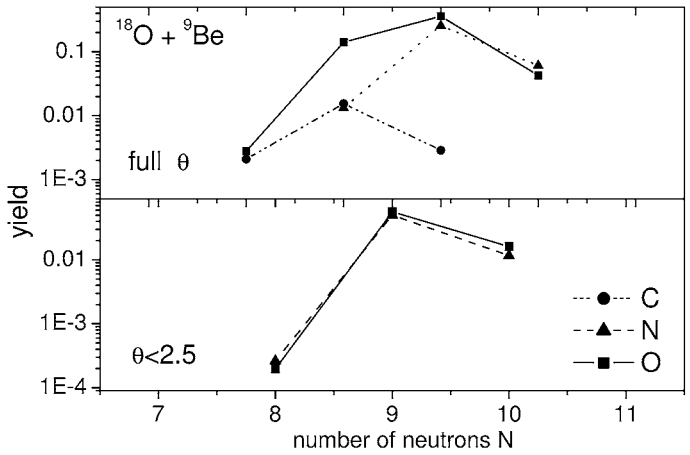

Fig. 5 – Calculated isotope distributions in the reaction $^{18}O + ^{9}Be$ for PLFs with $Z = 6, 7, 8$. Upper panel: distributions for all forward angles; lower panel: distributions with the restriction of the experimental acceptance angle $\theta < 2.5°$.

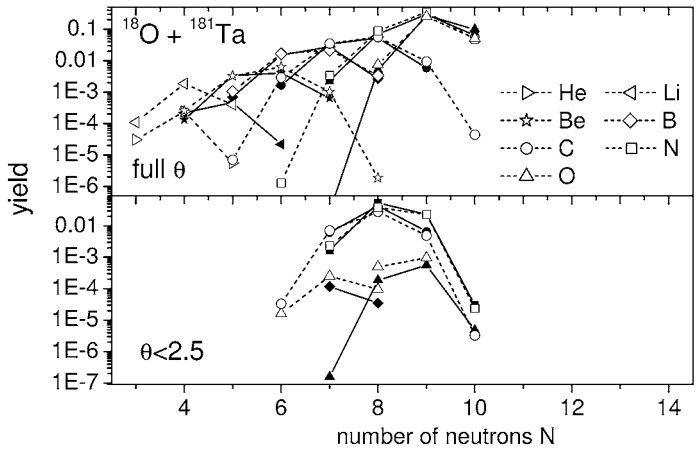

Fig. 6 – Isotope distributions for the reaction $^{18}O + ^{181}Ta$ for PLFs with $Z = 2$–8 as in Fig. 5. Results of calculations with 50 (dashed curves, open symbols) and 100 (solid curves, full symbols) test particles per nucleon are shown.

with fewer test particles, *i.e.* with more fluctuations, the distributions have the same mean values but a slightly larger width. This is what one expects as the effect of increased fluctuations.

We also study in more detail the velocities of the isotopes. As an overview we show in Fig. 7 the average velocity relative to the beam velocity of N ($Z = 7$) and C ($Z = 6$) fragments as a function of the impact parameter for the reaction $^{18}O + ^{181}Ta$. The results show the strong dependence of the velocity of the PLF on the impact parameter b: the more central the collision the smaller is the velocity of the PLF. For smaller values of the impact parameter the two nuclei interact longer and hence more energy is dissipated. One also sees in this figure that the velocity of the PLF fragment relative to the beam velocity in this deep

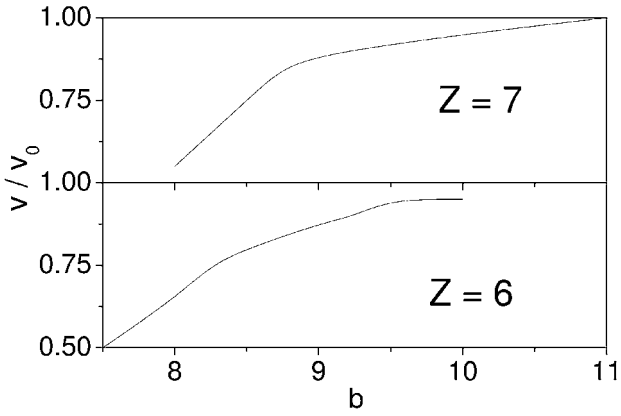

Fig. 7 – Mean velocity relative to the projectile velocity of C and N fragments as a function of the impact parameter b in the reaction $^{18}O + ^{181}Ta$.

inelastic collision reaches the value of one only for very large impact parameters and only for PLF close to the projectile (for $Z = 6$ it never reaches 1). Thus the dissipation is always present.

In Fig. 8 the velocity distributions for carbon isotopes in the reaction $^{18}O + ^{181}Ta$ are shown when calculated with and without angle restrictions, in the same way as for the isotope distribution in Fig. 6. It is seen that the mean velocity and even more so the width of the distribution changes strongly when the range of acceptance angles is restricted. For isotopes in the vicinity of the incident beam of ^{18}O with $N = 8, 9$ the value of the mean velocity coincides in the upper and lower part of the figure, while for $N = 7$ the mean value of velocity is considerably smaller and the distribution much wider, when no restriction is imposed. This might be of relevance because of statements in ref.[9] that in the calculated results in this paper the angle was limited to $\theta < 5°$ in order to have more statistics. This could have an influence on the distributions calculated, which will be discussed in more detail in comparison with experiment in the next section.

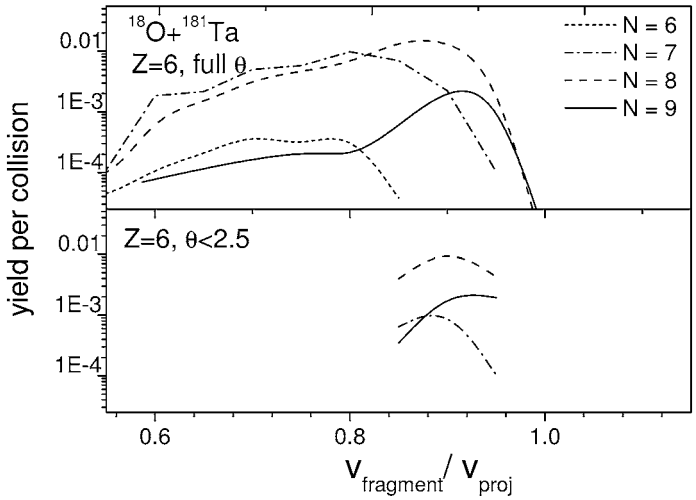

Fig. 8 – Yield of carbon ($Z = 6$) projectile-like fragments in the reaction $^{18}O + ^{181}Ta$ as a function of fragment velocity relative to projectile velocity. Upper panel: velocity distributions for all forward angles; lower panel: distributions with the restriction of the experimental acceptance angle $\theta < 2.5°$.

Altogether, our calculations show that the BNV method can describe deep-inelastic collisions of heavy ions. It reproduces well all known features of DIC: dependence of the widths and centroids of isotope distributions on impact parameter of the reaction, the dependence of the energy dissipated in the collision on the angle at which PLF is observed (Wilczynski plot). It also exhibits the important difference between the deflection curves for the reactions in inverse and normal geometry.

4. COMPARISON WITH EXPERIMENT AND DISCUSSION

As was mentioned in the introduction our investigation was motivated by the experimental results of Artukh *et al.* [9], where isotope and velocity distributions were measured at forward angles. The experimental velocity distributions are always characterized by a peak at $v/v_0 = 1$. In contrast it is seen in Figs. 7, 8 that the velocity distributions in our calculations always peak at values less than one, the more so, the smaller the mass of the PLF. However, the experimental distributions have an asymmetric shape with a long tail and sometimes even a slight shoulder for values below $v/v_0 = 1$. Thus it seems that two components might contribute to the data, as was also assumed in the higher energy data of Lahmer *et al.* [10].

The transport model according to the BNV approach is essentially a mean field approach which includes the averaged effect of two-body collisions. This is also implied by the use of a one-body phase space distribution function, and the method of using many test particles per nucleon. As discussed in the Introduction, in the Fermi energy regime the velocities of the nuclei as a whole and of the individual nucleons are of the same order. Therefore one should expect effects, where collisions of individual nucleons become important. These could be direct reactions, where only one or a few nucleons are involved, or more collective effects, like the abrasion, or shearing-off, of a larger part of the nucleus. It has sometimes also been called a breakup process [2], and is theoretically described in the Goldhaber model [11]. In this model it is assumed that the part of the projectile is abraded from the nucleus and the residual nucleus (PLF) continues to move with velocity close to beam velocity. The momentum distribution has the form of a Gaussian and the width is determined by the Fermi momentum of the abraded nucleus. It is given as $\sigma_p^2 = \sigma_0^2 A_F (A_P - A_F)/(A_P - 1)$, where σ_0 is about (90 MeV/c), and where A_F and A_P are the fragment and projectile masses, respectively [11, 13]. The corresponding width of the velocity distribution is then given as $\sigma_v^2 = \sigma_p^2/(2E_0 m_n A_F^2)$.

To compare the results of our calculations to the experiment we separated the contribution of the direct breakup and DIC processes in the velocity distribution. To do this we used a simple procedure, which is demonstrated in Fig. 9: we fitted the above-beam-velocity (right) part of the experimental velocity distribution with a gaussian with the center in the maximum of experimental distribution and a width, which fitted the experimental curve in the vicinity of $v/v_0 = 1$ and above. The residual yield below $v/v_0 = 1$ then represents the contribution of the DIC process.

In this way we also extract the width of the contribution at $v/v_0 = 1$ for different isotopes, which we compared to the Goldhaber formula given above. The

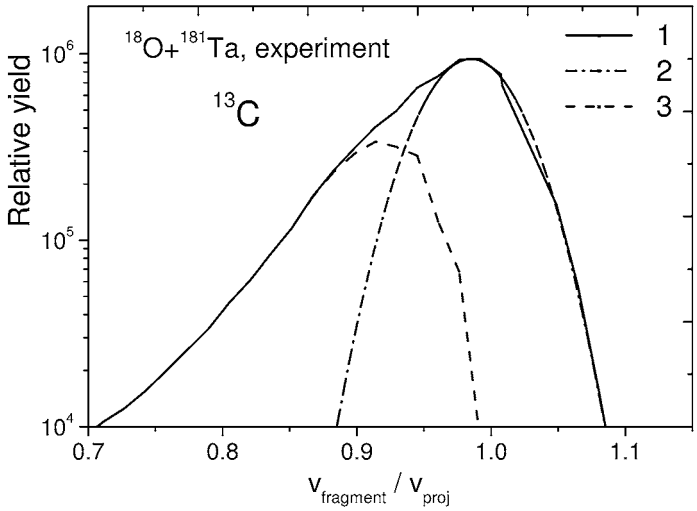

Fig. 9 – Decomposition of the experimental velocity distribution for ^{13}C fragments in the reaction ^{18}O + ^{181}Ta of ref. [9]: curve 1 (solid) experimental velocity distribution, curve 2 (dash-dot) fitted breakup contribution; curve 3 (dashed) residual dissipative contribution (see text).

results of our comparison are as follows: for the three isotopes ^{13}C, ^{15}N and ^{16}O the ratios of the extracted widths of the velocity distributions are $\sigma_O/\sigma_N/\sigma_C = 1/1.43/1.9$. The Goldhaber expression for the velocities gives $\sigma_O/\sigma_N/\sigma_C = 1/1.26/1.75$. For the σ_0 parameter for ^{16}O we obtain 54 MeV/c, which is smaller than the value quoted above [13]. However, in ref. [10] also a smaller width of about 60 MeV/c is obtained. Also the width of distribution increases with decreasing fragment mass faster than in the Goldhaber model. A possible explanation is that the lighter fragments are formed not only in the direct process but also by de-excitating of the heavier ones, which should increase the width of the distribution further.*** For some of the lighter PLF (*e.g.*, B and Be) the fitting with a gaussian is also possible; *e.g.* for ^{12}B it gives $\sigma_O^2/\sigma_{Be}^2 = 1/2.0 - 1/2.6$, where the uncertainty is due to lower statistics. The corresponding Goldhaber value is 1/2. From the peak position and from the close agreement of the widths ratios we conclude that the experimental spectra indeed contain contributions from two different modes: the gaussian part with the center at beam velocity corresponds to a break-up process and the contribution at lower velocities has its origin in deep inelastic collisions. It is this part that is compared to our calculations. The more abundant component is the direct break-up mode.

The ratio of these two modes is different for different isotopes. In the cases in which we decomposed the velocity distribution we determined the following ratios: $N_{DIC}/N_{bu} = 0.45,\ 0.31,\ 0.39,\ 0.45,\ 0.51$ for ^{11}Be, ^{12}B, ^{13}C, ^{15}N, ^{16}O,

respectively, (here N_{bu} is the break-up component with the velocity close to projectile velocity).

In Figs. 10, 11, and 12 a comparison of the theoretical and thus determined experimental DIC contributions is shown for carbon, nitrogen and oxygen isotopes, respectively. *E.g.* in Fig. 10 the velocity distributions are shown for carbon isotopes with neutron numbers 7, 8, and 9. The inset shows the experimental velocity distributions for $N = 7$ and the extracted breakup contribution. In the main panel the experimental DIC component is compared to the results of calculations for several isotopes. Here both the theoretical calculations and the experimental DIC component are normalized to the number of events for one collision, as in Fig. 13 later on.

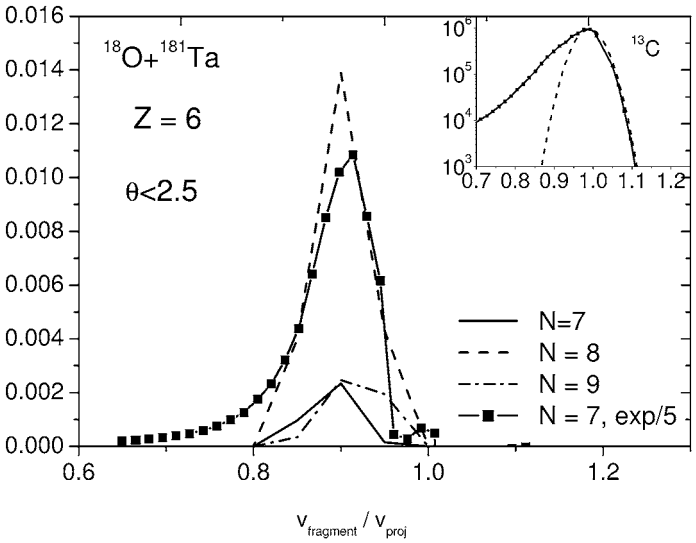

Fig. 10 – Yield of carbon fragments as a function of fragment velocity relative to projectile velocity in the reaction $^{18}O + ^{181}Ta$: The inset shows the experimental velocity distributions for ^{13}C, $N = 7$ (solid) and the fitted breakup contribution (dashed). The difference is the experimental DIC component. The main panel shows this experimental DIC component (squares, solid curve) compared to the results of the calculations for C fragments with $N = 7, 8, 9$. Calculated curves and experimental component in the main panel are normalized to yield per collision.

One sees from Figs. 10 to 12 that the centroids of the velocity distributions coincide quite well for theoretical and experimental results. The total ratio of calculated to the experimental yields is different in the different cases ^{13}C, ^{15}N, ^{16}O, as is evident by comparing the three figures. This shows that isotope distributions obtained in our calculations do not completely coincide with the experimental results of ref. [9].

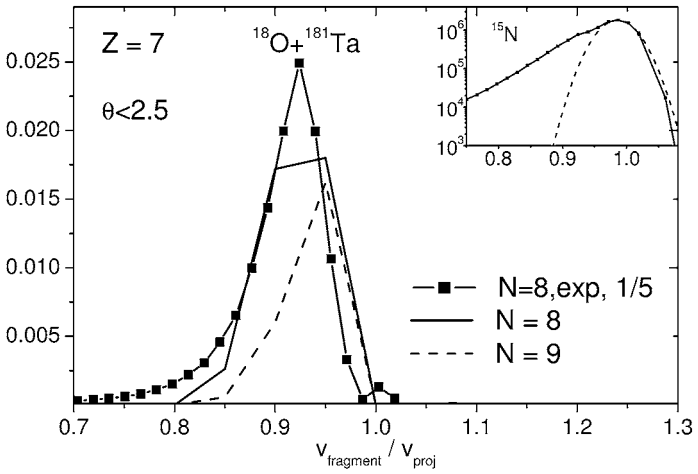

Fig. 11 – Velocity distributions for nitrogen isotopes as in Fig. 10.

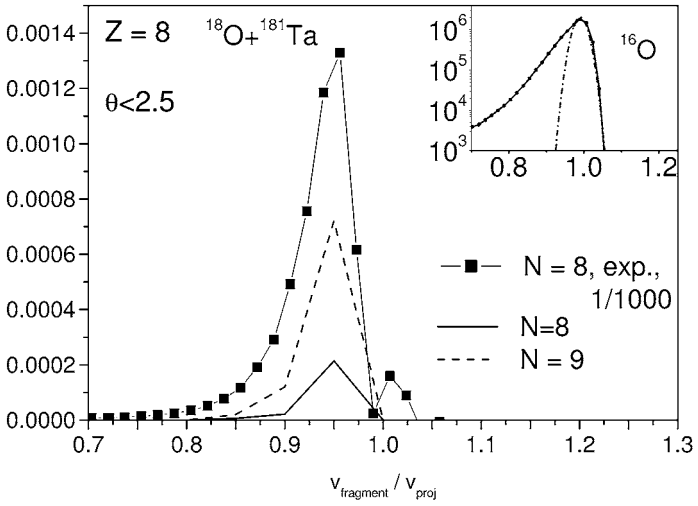

Fig. 12 – Velocity distributions for oxygen isotopes as in Fig. 10.

In Fig. 13 we show the fragment mass yield for impact parameters up to b = 13 fm, which are calculated here without acceptance angle restrictions. For the experimental acceptance angle ($\theta < 2.5°$) our calculations yield charge and isotope distributions which are much narrower than those seen in the experiment (cf. Figs. 5, 6). The solid and dotted curves show the results of calculations with 100 and 50 test particles per nucleon, respectively, and the dashed curve represents experimental data. In Fig. 13 we have normalized both the calculated and the experimental distributions to total yield equal unity; thus this represents the yield per collision. It is seen that the calculations give more heavy and fewer

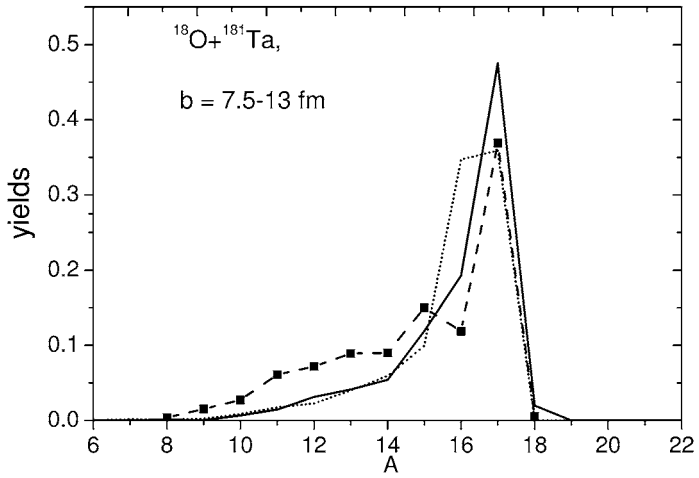

Fig. 13 – Projectile-like fragment mass yield in the reaction ^{18}O + ^{181}Ta: Dashed curve: experimental yield at forward angles ($\theta < 2.5°$); solid and dotted curves: theoretical results with 100 and 50 test particles per nucleon, respectively, in the full angular range. All distributions are normalized to unit total yield.

light fragments relative to the experiment. The number of test particles influences the mass distribution for the heavier fragments with loss of only a few particles, where it should be more sensitive to fluctuations.

Several comments are in order: The fact that our isotope distributions are too narrow could be interpreted as that our calculations contain too little fluctuations. Changing the number of test particles by a factor of two, changes the widths somewhat, but not sufficiently. Fluctuations, which are initiated by entire nucleons – and not by test particles – would be necessary to obtain larger widths. It is interesting to notice, that the QMD calculations in ref. [9] seem to give better widths.

Also, here we compare the primary fragments obtained in our calculation with the final, cold fragments measured in the experiment. As discussed above, an evaporation code should be linked to the transport codes to describe the deexcitation. In this process the excited fragments would evaporate nucleons and light clusters and would thus be expected to reduce the higher and increase the lower part of the mass distribution. This was investigated in the calculations of ref. [9], where the effect there was not very substantial.

Finally, we compare the total experimental mass yields with our calculations, which only contain the dissipative component. We discussed above that the ratio of the dissipative to the direct component is not the same for different isotopes, and this will distort the mass distribution.

5. CONCLUSION

The aim of the work was to study whether deep-inelastic or dissipative collisions in the Fermi energy domain can be described with modern, high precision transport calculations of the BNV (or BUU) type. We find that our approach describes many characteristic features of dissipative collisions: deflection curves with Coulomb and nuclear rainbows, angle-energy loss correlations (Wilczynski plots), fragment yields and energy spectra, peaked at velocities below beam velocity.

We compared these calculations to recent experimental data for the collisions $^{18}O + ^{9}Be$, ^{181}Ta at 35 AMeV [9, 8], which were measured at extreme forward angles. From the deflection curves we see, that the range of impact parameters that contributes to the forward angle projectile-like yield is very different in the two reactions, and thus we demonstrate the very different situation of inverse and normal kinematics. Only the heavier system is expected to contain substantial dissipative contributions. We find that the isotopic distributions agree reasonably well with respect to the maxima of the distributions, but have too narrow widths. However, in the calculations we consider the primary fragments after freeze-out, which are still excited. The de-excitation by evaporation of light particles should lead to bigger widths, which has not yet been included.

The isotopically separated velocity distributions, however, appear very different from the data, since the experimental distributions are always peaked at beam velocity in contrast to the calculations, which peak at lower velocities consistent with the energy loss observed in a dissipative collision. To explain this we interpret the data as containing two components: a direct fragmentation or breakup component at beam velocity and a dissipative component. We extract the direct component by a Gaussian fit to the high velocity part of the distribution and attribute the residual to the dissipative process. This is a similar approach as was used in an earlier work by Lahmer *et al.* [10] in a different system.

The direct fragmentation component is described here in the Goldhaber model [11] as an abrasion process. The model agrees well with the extracted component with respect to the dependence of the width of the distribution for different isotopes. The dissipative component, on the other hand, is described well with respect to the position and width by our transport calculations. The relative contributions of the two components and of the dissipative components of different isotopes has to be understood better, however. Generally, it is of considerable interest, that a semiclassical transport approach does not contain the direct fragmentation component.

Thus we believe that transport calculations can contribute to understand better the mechanism of heavy ion collisions in the Fermi energy domain. They could thus be used for further studies, *e.g.* also of the symmetry energy below

saturation density, and generally serve as a powerful tool in explaining and planning future experiments of low-energy peripheral heavy ion collisions.

Acknowledgements. We would like to thank Profs. V. Baran, M. Zielinska-Pfabe, A. G. Arthuk, I. N. Mikhailov, V. V. Pashkevich and W. von Oertzen for very helpful discussions, and V. B. especially for the use of his codes. T. M. would like to thank the LNS in Catania and the University of Munich for warm hospitality, and Dr. S. Kimura for continued support. T. M. also expresses thanks to the Department of Theoretical Physics of IPNE, Bucharest, and particularly to Dr. Silisteanu, for making it possible to attend the conference and present this report.

REFERENCES

1. J. Wilczynski, Nuclear molecules and nuclear friction, *Phys. Lett.*, **B47** (1973) 484.
2. H. Fuchs, K. Moehring, Heavy-ion break-up processes in the Fermi energy range, *Rep. Prog. Phys.*, **57** (1994) 231.
3. U. Schroeder, J. R. Huizinga, Damped nuclear reactions, *Treatise on Heavy-Ion Science* Vol. 2, ed. A. Bromley, Plenum, New York, 1984, p. 113.
4. R. Beck, D. H. E. Gross, H. Kalinowski, Proc. Int. Conf on Nuclear Physics (München 1973) contribution 195, ed H. J. Mang *et al.*, Amsterdam: North-Holland, 1973.
5. A. Lukasiak, W. Nörenberg, *Z. Phys.*, **A326** (1987) 79.
6. G. F. Bertsch, S. Das Gupta, A guide to microscopic models for intermediate energy heavy-ion collisions, *Phys. Rep.* (1988) 189.
7. M. F. Rivet *et al*., Dynamical aspects of violent collisions in $Ar + Ag$ reactions at E/A = 27 MeV, *Phys. Lett.*, **B215** (1988) 55.
8. A. G. Artukh *et al.*, Some regularities in the beam-direct production of isotopes with $2 < Z < 11$ induced in reactions of ^{18}O (35 A MeV) with Be and Ta, *Nucl. Phys.*, **A701** (2002) 96c.
9. A. G. Artukh *et al.*, QMD approach in description of the $^{18}O + {}^{9}Be$ and $^{18}O + {}^{181}Ta$ reactions at E_{proj} = 35 AMeV, *Acta Physica Polonica*, **37**, 1875 (2006).
10. W. Lahmer *et al.*, Transfer and fragmentation reactions of ^{14}N at 60 MeV/u, *Z. Phys.*, **A337**, 425–437 (1990).
11. A. S. Goldhaber, Statistical model of fragmentation processes, *Phys. Lett.*, **53B**, p. 306–308 (1974).
12. H. Utsonomiya, "Stripping" reaction in heavy ion projectile dissociation: Extended Serber model, *Phys. Rev.*, **C32** 849 (1985).
13. C. K. Gelbke *et al.*, Influence of intrinsic nucleon motion on energy spectra and angular distributions for ^{16}O-induced reactions at 20 MeV/A, *Phys. Lett.*, **70B**, p. 415–417 (1977).
14. Y. Abe *et al.*, On stochastic approaches of nuclear dynamics, *Phys. Reports*, **70B**, 49–196 (1996).
15. V. Baran, M. Colonna, V. Greco, M. Di Toro, *Phys. Rep.*, **410**, p. 335 (2005).
16. P. G. Reinhard, E. Suraud, On dissipative features of the Vlasov equation, *Ann. Phys.*, **239**, 293 (1995).
17. J. Blocki, Y. Bohen, J. R. Nix, M. Robel, A. J. Sierk, W. J. Swiatecki, One-body dissipation and super-viscosity in nuclei, *Ann. Phys.*, **113**, 330–86 (1978).
18. L. G. Moretto, R. P. Schmitt, Deep inelastic reactions: a probe of the collective properties of nuclear matter, *Re. Prog. Phys.*, **44**, 533–591 (1981).